

# Design of Coplanar Stripline Bandpass Filter with Re-configurable Filter Switch

Banani Basu<sup>1</sup>, Edison Kho<sup>1</sup>, and Arnab Nandi<sup>1</sup>

<sup>1</sup>National Institute of Technology Silchar

March 29, 2024

## Abstract

This paper has designed a bandpass filter using a coplanar stripline stub (CPS) resonator consisting of open and short-ended strip lines connected to the PIN Diode switches. The use of spurline stub resonators inside CPS results in bandpass and bandstop filters, depending on the PIN diode switch configurations. The work presents a novel circuit architecture aimed at reducing parasitic resonance of the spurline resonators and acquire the necessary series stub characteristics. The proposed filter resonates at 6.9-9 GHz and 1.7-4.7 GHz, and 8.4 GHz when the PIN diodes are forward and reverse-biased, respectively. It also resonates at 1-2.1 GHz, 4.8-5.3 GHz, and 6.9-9 GHz when one diode is reverse-biased, and the other is connected in forward bias. An insertion loss below -0.55 dB and a return loss less than 10dB have been obtained during simulation and measurement. The designed filter can find different applications for the 1.8 GHz GSM band, 2.4/5.8GHz (WLAN), 3.6 GHz (WiMAX), Long Term Evolution (LTE), and WIFI. The filter can be used in various multi-frequency systems owing to its compact size. The measured and simulated findings of the proposed CPS spurline stub resonator wideband bandpass filters are substantially consistent.

**ARTICLE TYPE**

# Design of Coplanar Stripline Bandpass Filter with Re-configurable Filter Switch

Edison Kho<sup>1</sup> | Banani Basu<sup>2</sup> | Arnab Nandi<sup>3</sup>

<sup>1,2,3</sup> Department of Electronics and Communication Engineering, National Institutes of Technology Silchar, Silchar, Assam, Pin 788010, India.

**Correspondence**

Banani Basu, Department of Electronics and Communication Engineering, National Institutes of Technology Silchar, Silchar, Assam, Pin 788010, India. Email: banani@ece.nits.ac.in

**Abstract**

This paper has designed a bandpass filter using a coplanar stripline stub (CPS) resonator consisting of open and short-ended strip lines connected to the PIN Diode switches. The use of spurline stub resonators inside CPS results in bandpass and bandstop filters, depending on the PIN diode switch configurations. The work presents a novel circuit architecture aimed at reducing parasitic resonance of the spurline resonators and acquire the necessary series stub characteristics. The proposed filter resonates at 6.9-9 GHz and 1.7-4.7 GHz, and 8.4 GHz when the PIN diodes are forward and reverse-biased, respectively. It also resonates at 1-2.1 GHz, 4.8-5.3 GHz, and 6.9-9 GHz when one diode is reverse-biased, and the other is connected in forward bias. An insertion loss below -0.55 dB and a return loss less than 10dB have been obtained during simulation and measurement. The designed filter can find different applications for the 1.8 GHz GSM band, 2.4/5.8GHz (WLAN), 3.6 GHz (WiMAX), Long Term Evolution (LTE), and WIFI. The filter can be used in various multi-frequency systems owing to its compact size. The measured and simulated findings of the proposed CPS spurline stub resonator wideband bandpass filters are substantially consistent.

**KEYWORDS:**

Coplanar stripline, Series stub, Coplanar-strip resonator, PIN diode, RF switch, Re-configurable filter

## 1 | INTRODUCTION

The Coplanar stripline (CPS), unlike the coplanar waveguide (CPW) has no semi-infinite ground. So, the intended circuit can be reduced to fit into a smaller space<sup>1</sup>. As the CPS's uniplanar design is the most precise planar technology, the employment of series and shunt active passive elements is simple and may be implemented without the necessity of via-hole processing. Since 1975, CPS has been extensively researched and developed as a supplementary structure of the coplanar waveguide (CPW). A CPS band pass and band rejection filter has been designed using spurline stub resonators<sup>2</sup>. However, as the spurline resonators have a parasitic resonance, their use has been limited in CPS. With the introduction of the simple wire-bond or airbridge, the parasitic resonance is controlled, and the typical features of a perfect series stub are attained<sup>3</sup>. Meanwhile, the wire-bonds and airbridges require additional processing, which may deteriorate the circuit's quality and contribute to a source of loss. The DGS has been used at the ground plane to suppress spurious and harmonics frequency responses above the passband. Along with higher mode suppression, DGS reduces the front-to-back ratio, which in turn decreases the gain in the desired direction in the antenna due to defects in the ground plane<sup>4,5,6</sup>.

Over the past several decades, many studies have been proposed and conducted to design microwave antennas and filters using CPW<sup>7</sup> and CPS<sup>6,7,8,9</sup>. As described in<sup>6,8</sup> on a survey of analogous capacitances and inductances of distinct CPS discontinuities based on the method of moment together with Golerkins approach and duality concept. It has become an excellent choice for constructing low-cost uniplanar microwave circuits owing to the appearance of higher-order modes towards the exceeding edge of the interest frequency range. Balanced filters using CPS rather than slotline have recently been described with better Q factor on bandpass transmission differential mode, expanded upper stopband for DM low pass response, compact size and the first DM harmonic intrinsic suppression is presented in<sup>9</sup> and open-circuited CPS in<sup>10,11</sup>. In<sup>11</sup>, a coupled split-ring resonator to coplanar stripline has been demonstrated as a bandstop filter. A balanced CM suppression with a double-sided coplanar strip wideband is proposed in<sup>12,13</sup>. Three balanced microstrip-to-CPS transformations with excellent pure CM suppression and wideband DM filtering capabilities are presented in<sup>13,14,15</sup> and a miniaturized type of planar plasmonic waveguides with ultra-wideband filtering performance has been reported in<sup>16</sup>. The PIN diode modeling for re-configurable filters<sup>17,18</sup> and antenna<sup>19,20</sup> are integrated to form a multi-band operating filter. A compact single/multi-band coupled-multiline filtering unit has been proposed to design RF filtering devices<sup>21</sup>. The compact size and multiple operational bands and order make CPS technology an attractive alternative for circuit design in appliances such as mixers, antennas<sup>22,23,24</sup>, and filters<sup>25</sup>.

This paper presents the re-configurable CPS bandpass filter with PIN diodes. The PIN diodes are linked in series through a gap in the inner spurline conductor and the CPW inter-digital connection has converted the bandpass filter to a spurline stopband filter. When the spurline stub is short-circuited by forward biasing the PIN diode, it behaves as a stopband filter and resonates at 6.7-9.1 GHz. On the contrary, when the reverse biased state of the PIN diode is considered, it acts as a passband and resonates at 1.7-4.7 GHz and 7.4-9 GHz, whereas one of the diodes is made forward biased and the rest as reverse-biased it resonates at tri-bands from 1-2.1 GHz, 4.8-5.3 GHz, and 6.9-9 GHz. It has utilized the CPS strip oriented at an angle of 45° relative to the original horizontal position, which causes realignment of the E-and H fields to reduce the coupling and cross talk. The diagonal orientation of fields has limited the radiation in a specific direction and offered better filtering effects. The enlarged stub width has increased the capacitance lowered the resonant frequency, and suppressed the parasitic modes. The proposed filter offered a higher selectivity of up to 37 dB in the lower and upper bands which is significantly higher than that of the reported values presented in<sup>2,3,12,13</sup>. Without wire bonds or air bridges, the structure has offered wider bandwidth and prohibited the parasitic modes. The proposed design is small in size and offers 2<sup>nd</sup> and 3<sup>rd</sup> filter response, an in-band insertion loss of 0.5 dB, RL up to 13 dB, and FBW of 110%.

## 2 | CONSTRUCTION OF BANDPASS FILTER

Figure 1 (a) shows the construction of the bandpass filter using CPS spurline stub resonators. The section has described the construction and measurement of the CPS structure and CPS spurline stub resonator slot.

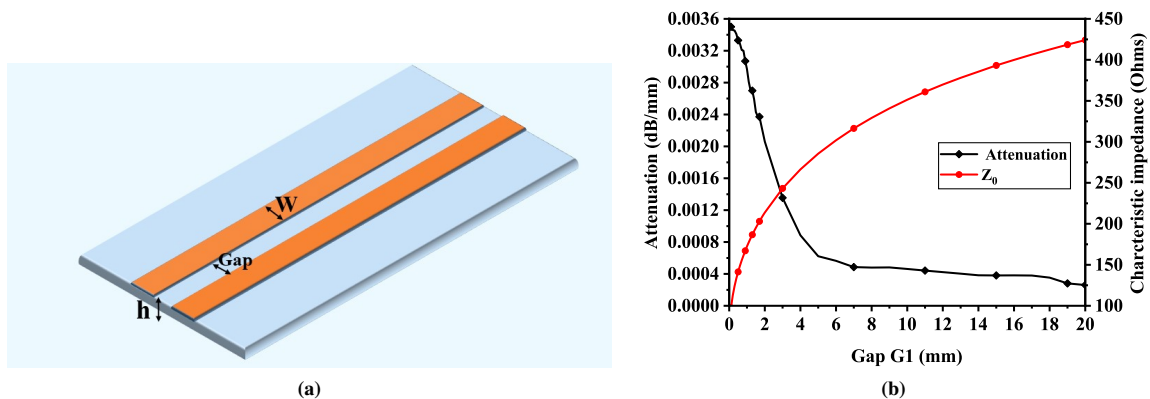


**FIGURE 1** Basic Co-planar (a) CPS geometry (b) Variation of Attenuation and Characteristic Impedance with gap.

## 2.1 | Analysis of CPS characteristics

As shown in Figure 1(a), the width  $W$  and partition between the strips (Gap)  $G1$  are set at 2 mm and 0.2 mm, respectively. The RT/Duroid 5880 substrate is utilized to design the circuit having a  $35 \mu\text{m}$  thick copper layer, 0.787 mm substrate height ( $h$ ), and 2.2 dielectric constants ( $\epsilon$ ).<sup>1</sup> Describes analytical procedures for estimating the effective dielectric constant, characteristic impedance<sup>7</sup>, and dielectric and conductor losses of the CPS<sup>11,12</sup>. The study takes into account the quasi-TEM closed-form characteristics of the CPS on a fixed substrate height. The loss mechanisms studied in this research consider dielectric  $\alpha_d$  and conductor  $\alpha_c$  losses. Overall attenuation and characteristics impedance considering dielectric and conductor losses for different separation gaps varying from 0.1 to 20mm and fixed strip width  $W=2$  mm at 10 GHz are plotted in Figure 1. It is observed from Figure 1(b) that the wider separation gap lowers the overall attenuation  $\alpha_d + \alpha_c$  and increases characteristic impedance  $Z_0$ .

## 2.2 | Analysis of CPS spurline stub Resonator slot

The CPS strip is slanted by  $45^\circ$ , followed by cutting the stub resonator on the CPS strip. The stub width  $W1$  is enlarged, and finally, the PIN diodes are inserted into the open gap resonator. The details of this implantation are described in Figure 2. As in Figure 3, we have constructed the couple lines with slot  $G1$ , length  $L1$ , and width  $W$  on both sides. Then the lines are slanted by an angle of  $45^\circ$  and have a slant length of  $L2$ . Slanting has increased the slot gap between a couple lines to  $G2$ . The slanted lines re-joined with the couple lines of length of  $L3$ . The stub width ( $W1$ ) changes the electrical length, which strategically affects the resonant frequencies. By carefully choosing the width of the stub, we have controlled and mitigated undesirable resonances, increasing the overall filter efficiency as in Figure 4.

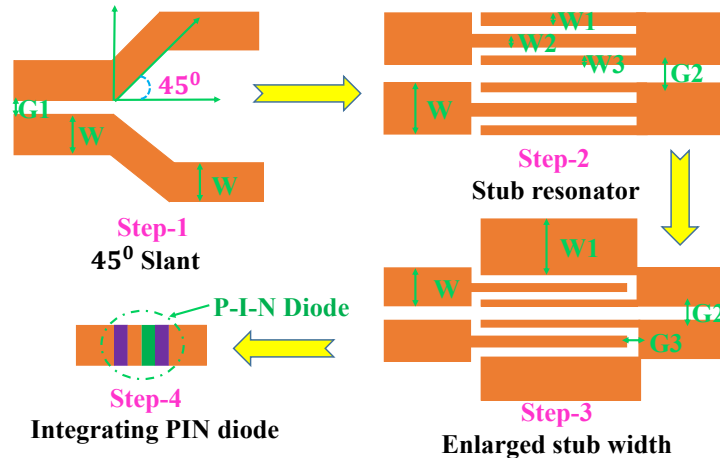
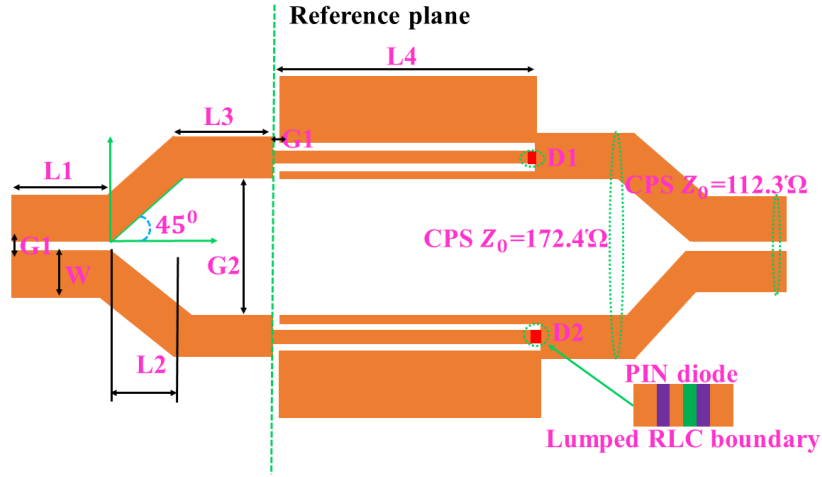


FIGURE 2 Systematic design approach of the CPS filter

At the center, a spurline stub resonator is designed consisting of a series of open-ended and short-ended spurline stub structures, as shown in Figure 3. The open-ended series spurline stub resonator of length  $L4$  is optimized to resonate at the desired operating frequency. The short-ended stub with length  $L5$  is placed below it and connected through a PIN diode switch. The dimensions of the CPS structure are rigorously optimized to obtain the desired frequency response and are listed in Table 1.

The open-ended series spurline resonator behaves as an inductor. The coupling capacitance arises due to the interaction with the CPS spurline stubs and varies with the gap  $G1$ . Moreover, narrower  $G2$  provides highly loaded  $Q_L$  and low loss. CPS attenuation decreases as the CPS gap separation  $G1$  increases, as analyzed and depicted in Figure 1(b). Thus, narrowing the  $G2$  and widening the  $G1$  impact the  $Q_L$  significantly. Unloaded  $Q_U$  and loaded  $Q_L$  values for various  $G1$  and  $G2$  are calculated



**FIGURE 3** Structure of CPS filter with PIN diode

**TABLE 1** Dimension(mm) of the CPS structure

| Parameter | Value | Parameter | Value              | Parameter | Value | Parameter | Value |
|-----------|-------|-----------|--------------------|-----------|-------|-----------|-------|
| L1        | 6     | L4        | 12                 | W         | 2     | W3        | 0.3   |
| L2        | 1     | L5        | 11.7(Open Circuit) | W1        | 2.3   | G1        | 0.2   |
| L3        | 4     | L5        | 12 (Short Circuit) | W2        | 1     | G2        | 1     |

using the HFSS EM simulator and plotted in Figure 5 . Table 2 shows that the wider G2 yields a higher  $Q_L$  value, but  $Q_U$  remains nearly the same when G1 is set at 0.2mm. Eq. 1 and 2 calculate the  $Q_U$  and  $Q_L$  values of the band-stop resonator.

$$Q_U = \frac{Q_L}{\sqrt{1 - 2 \times 10^{-\left(\frac{L}{10}\right)}}} \quad (1)$$

$$Q_L = \frac{f_0}{\Delta f_{3dB}} \quad (2)$$

where  $f_0$  and  $\Delta f_{3dB}$  denote center frequency and 3-dB insertion loss bandwidth respectively.

The  $Q_U$  and  $Q_L$  values of the series spurline stub resonator's are measured as 137.1 and 137.8, respectively, as the dimension of G1 and G2 is set at 0.2mm and 1 mm. The 3-dB insertion loss bandwidth is found to be 0.85 GHz, and the IL becomes -0.57 dB at center frequency 3.3 GHz (% of BW 18.9%) in the reverse biased state of the PIN diode. -0.34 dB insertion loss is obtained at center frequency 7.1 GHz (% BW 133%) during the forward biased condition of the PIN diode.

**TABLE 2** Loaded and unloaded Q-factors:  $Q_L$  and  $Q_U$

| G1 (mm) | G2 (mm) | $Q_L$  | $Q_U$  |
|---------|---------|--------|--------|
| 0.2     | 0.2     | 121.25 | 121.27 |
| 0.2     | 0.5     | 129.7  | 130.6  |
| 0.2     | 1       | 136.1  | 137.4  |

The simulated  $Q_L$  and  $Q_U$  values of the PIN diodes are 121.25 and 121.27, respectively, for the forward-biased condition and reduce to 76.25 and 77.27 at the reverse-biased state. In an ideal TL model, 0 dB IL corresponds to infinite  $Q_U$  ensuring

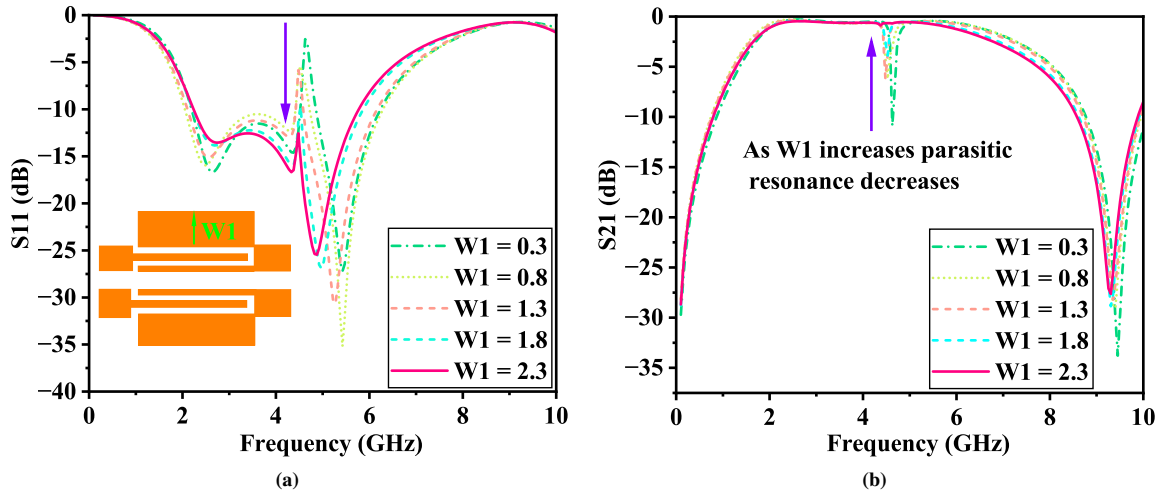


**FIGURE 4** Scattering parameters as the stub width  $W_1$  increases (a) Variation in reflection coefficient and (b) Variation in parasitic resonance as  $W_1$  increases.

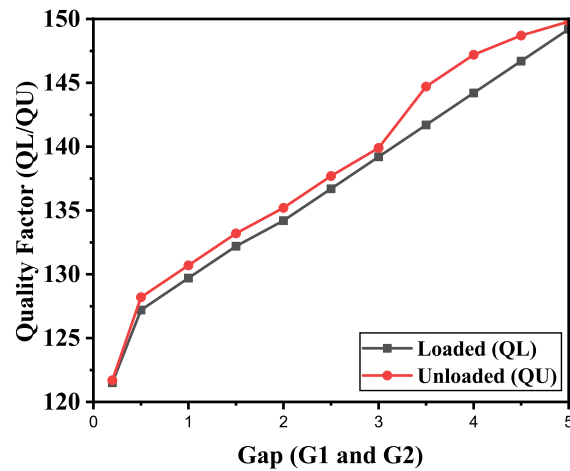


**FIGURE 5** Quality factor for different  $G_1$  and  $G_2$

flawless transmission. It is observed that increasing the width ( $W$ ) and  $G_1$  leads to a decrease in  $Q_U$  and a rise in  $Q_L$ , according to the observed pattern, which finally leads to higher IL and narrower bandwidth.

### 3 | DESIGN OF CPS FILTER

Figure 3 depicts the configuration of a CPS spurline-stub bandpass filter. This spurline is useful when  $W$  is large and slot  $G_1$  is tiny. CPS short-ended and open-ended series spurline resonators have been theoretically and experimentally demonstrated in the section. The serially connected open-ended stub limits the signal over non-resonant frequencies yet permits it at resonant frequencies. As depicted in Figure 3, the corresponding circuit design functions as a series-connected, open-ended stub with differential length at the two terminal transmission lines. However, as the reference plane is shifted by the distance  $G_1$  along the slot's borders, the transmission line length approximates  $L_4$ , which represents a single spurline resonator as a single element bandpass filter. Lumped equivalent element circuits have been derived from the scattering parameters to model the discontinuities.

### 3.1 | Band stop filter

A standard CPS line splits into three smaller lines that rejoin after a quarter wavelength distance, as presented in Figure 3. The short-circuit series stub acts as a series inductor with parasitic elements on the transmission line. In this condition, an RF current passes around at the slot's terminating end, storing the magnetic energy, which induces inductive reactance, as shown by  $L_2$  in Figure 6(a). In bandstop filters, the length of the stub is chosen equal to  $(\lambda/4)$  corresponding to the stopband frequency, and thus, at resonance, the stub prohibits RF power from approaching the load. However, in the proposed design, the stub length has been considered even less than  $(\lambda/10)$  while using additional inductors to maintain the same stopband frequency. The values of the inductors are suitably tuned by adapting the length and width of the inner conductor between the stubs, as presented in Figure 6. The gap between the triple lines is calculated precisely to fine-tune the rejection frequency. The smaller the gap, the narrower the stopband. However, it is observed that the filter frequency response is negligibly affected by the slot gap between the input CPS line and the open-circuited line of the coupler.

### 3.2 | Wideband Bandpass filter

As an ultra-wideband bandpass filter, an open-ended spurline stub resonator is implemented. When the two strip conductors are connected in an open circuit, a fringing electric field induced a capacitive reactance, which can be modeled as a lumped capacitance  $C_1$  and  $C_2$ . The CPS spurline stub having a gap of length  $G_3$  as shown in Figure 6(b). This gap may be represented as a lumped Pi-network with  $C_1$  and  $C_2$  fringing capacitance's and a coupling  $C_3$  capacitance. The analogous circuit of the open-end CPS Spurline stub resonator is modeled as an series stub stepped impedance open-circuit, as shown in Figure 6(b). The open-circuit series stub in the center conductor is modeled as a capacitor with parasitic elements connected in series with the transmission line. As the length of the center open stub is set at  $\lambda/4$ , the stub acts as a band- pass filter. The length of central conductor is typically kept less than  $\lambda/10$  and composed of the additional capacitance chosen based on the stub length and the slot width.  $G_3$  can be used to change the open-ended notch frequency in spurline stub. The stepped impedance stub resonator<sup>3</sup> can also explain this variance. Schematic diagram of an equivalent CPS filter structure, as obtained from ADS using a microstrip coupled line employing a cascaded transmission line configuration of the high and low impedance, is shown in Figure 4. Because these transmission lines are substantially shorter than the corresponding guided wavelength, they function as semi-lumped elements. Higher-impedance lines function as series inductors, whereas lower-impedance lines function as shunt capacitors. They are converted into respective LC equivalent using circuit transformation. As a result, this filter construction closely matches the LC ladder-type bandpass filters shown in Figure 6.

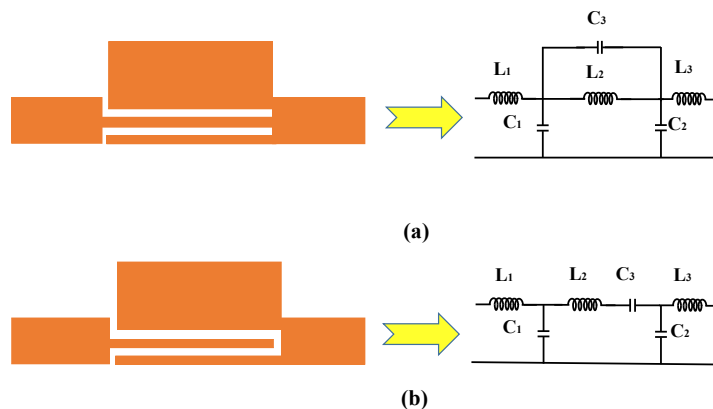


**FIGURE 6** The structure and equivalent circuit of Series CPS Spurline Resonator (a) Short-ended (b) Open-ended

Figure 6 presents the structures and equivalent circuits of short and open-ended CPS spurline resonators as in<sup>12</sup>. The filter construction closely matches the LC ladder-type bandpass filters. the equivalent load impedance in open-ended cases is presented in Eq.(3)

$$Z(\omega) = j\omega L_1 + \frac{1}{j\omega C_1 + \frac{1}{j\omega L_2 + \frac{1}{j\omega C_3} + \frac{1}{j\omega C_2 + \frac{1}{j\omega L_3}}}} \quad (3)$$

So, for the open-ended case, the resonant frequency  $f$  is represented as

$$f = \frac{1}{2\pi} \sqrt{\frac{L_2 C_1 (2C_3 + L_2 L_3)}{C_2 L_1 (C_2 + 2L_2 L_3)}} \quad (4)$$

**TABLE 3** Lumped L(nH) and C(pF) values

| Closed-ended spurline stub resonator | Open-ended spurline stub resonator |
|--------------------------------------|------------------------------------|
| C1=0.016                             | C1=75                              |
| C2=1.35                              | C2=0.4                             |
| C3=1.62                              | C3=2                               |
| L1=3.157                             | L1=2                               |
| L2= 2.123                            | L2=5                               |
| L3=2.237                             | L3=3.5                             |

The values of capacitances  $C_1, C_2, C_3$  and inductances  $L_1, L_2, L_3$  as while as the stub length  $L_4$  are calculated using ADS keysight software. The units of stub length  $L$  are in mm, whereas the capacitance and inductance units are in pF and nH. Table 3 lists the Lumped LC values in closed and open-ended spurline stub resonators obtained using ADS software which offers the resonating frequency at 4.20 GHz.

## 4 | METHOD OF ELIMINATION OF PARASITIC RESONANCE

In order to comprehend the parasitic resonance, we refer to the current distribution of the CPS filter as shown in Figure 7 . As the spurline stub resonator is considered a CPS series line, the current flowing through the inner resonator conductor must be in the reverse direction concerning that of the two outer parallel resonator conductors. The current distribution through the resonator, as in Figure 7 , confirms the presence of the parasitic mode as in<sup>3</sup>, which is further suppressed by implementing the following two methods (a) Slanting the CPS structure and (b) Enlarging the CPS spurline stub width.

### 4.1 | Slanted design on CPS

The CPS structure is slanted on either side of the design at  $45^\circ$ , as shown in Figure 2 . The slanted CPS structure corresponds to high impedance along with minor degradation in insertion loss but retains the return-loss response better than -10 dB over the entire bandwidth of interest.

The CPS structure is slanted on either side of the design at  $45^\circ$  in this paper as shown in Figure 2 . The slanted CPS contributes a low-loss, ultra-wideband way for connecting various bandwidth components. In both experimentally and simulation studies, the slanted transition approaches were shown to reduce overall attenuations by shifting from a tiny device-constrained to a low-loss transmission line and providing slanted design instructions with minimum influence on propagation. Longer slants can be investigated, but this is counterproductive because shorter slants are preferred. This CPS structure which is slanted corresponds

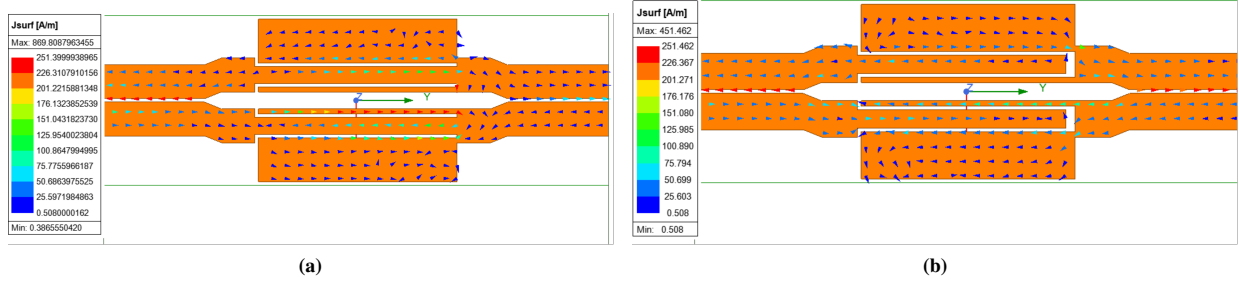


**FIGURE 7** Current distribution on CPS spurline stub resonator for (a) Short-ended (b) Open-ended

to the high impedance value. Despite the high impedance value, there is minor insertion loss degradation and the response of return-loss remained better than -10 dB.

## 4.2 | Enlarging the CPS stub width

The CPS has certain extra benefits over the CPW as it removes the need to create air bridges around discontinuities to suppress the undesirable mode. As mentioned in<sup>3</sup>, the crossover connections between the ground planes are required to suppress the spurious modes but are perturbed by the CPW model. Freestanding junctions, known as air bridges, have long been a feature of classical microwave CPW technology. Still, the fabrication procedure of the same on superconductive microwave circuits is tedious and creates additional complexity to the circuit, which sometimes reduces its performance, as well as itself, may become a source of loss. The disadvantage of wire-bond is that the structure requires several crossings across the resonator, which gradually reduces the quality factor at both low and high powers. This loss factor includes radiation, conductor, and dielectric losses. In<sup>2,3</sup> a wire bond method is used to eliminate a parasitic mode. In<sup>11</sup>, a double split-ring resonator, and in<sup>13,14,16</sup> double-sided shunt-stub structure and SL-stub vertical coupling are used to suppress the spurious radiation. In<sup>2</sup>, for the odd mode, the circular open circuit is utilized to eliminate the parasitic mode, and for the even mode, a circular arrangement with a greater radius is utilized. In the proposed filter, we have increased the CPS stubs width  $W1$  on both sides of the CPS line to 2.5 mm. With the width  $W1$ , the capacitor value increases, reducing the resonant frequency. Moreover, the higher order mode current around CPS width flows towards a similar direction as in Figure 7. Thus, along with the suppression of the parasitic resonance, the bandwidth enhances as the width  $W1$  increases. For a short-ended CPS structure, the bandwidth is obtained from 6.9-9.4 GHz; for an open-ended, the bandwidth is achieved from 1.7- 5.9 GHz.

## 5 | IMPLEMENTING OF SWITCHING TECHNIQUES

The section has modeled the PIN diode switches operating at forward and reverse biased states. Figure 3 depicts the prototype filter, and its similar transmission model is presented in Figure 8. The switch is connected across the 0.5 mm gap in the coplanar stripline conductor. The PIN diode is biased with the external voltages to open and short the resonators. For simulation, NXP BAP65(03), 115 PIN diode is considered, which is represented as a combination of a 1.5 nH inductor linked in series to a resistor of 1 $\Omega$  in a forward-biased state, and modeled as a 1.5 nH inductor linked in series with the parallel combination of a resistor of 20 K $\Omega$  and the capacitor of 0.5 pF for the reverse-biased state. The equivalent circuit of the PIN diode switch in forward and reverse bias conditions is shown in Figure 9 (a) and (b). Here input impedance matching is achieved by adapting the capacitor  $C1$  and the inductor  $L$ . The forward biased state provides a short circuit that permits currents to flow toward the load. However, the model provides an open circuit phenomenon in the reversed biased state, thus blocking the current flow. The frequency reconfigurability is attained in the FB and RB states as it operates in four modes, each having a distinctive pattern of operating frequencies. States 1 and 2 operate at triband. State 3 operates at dual bands, and State 4 operates at the single band, the proposed CPS structure with an embedded PIN diode and its simulation results for the different diode states are plotted as shown in Figure 13. The conditions of the PIN diodes for different state and respective operating frequency bands are briefed in Table 4.

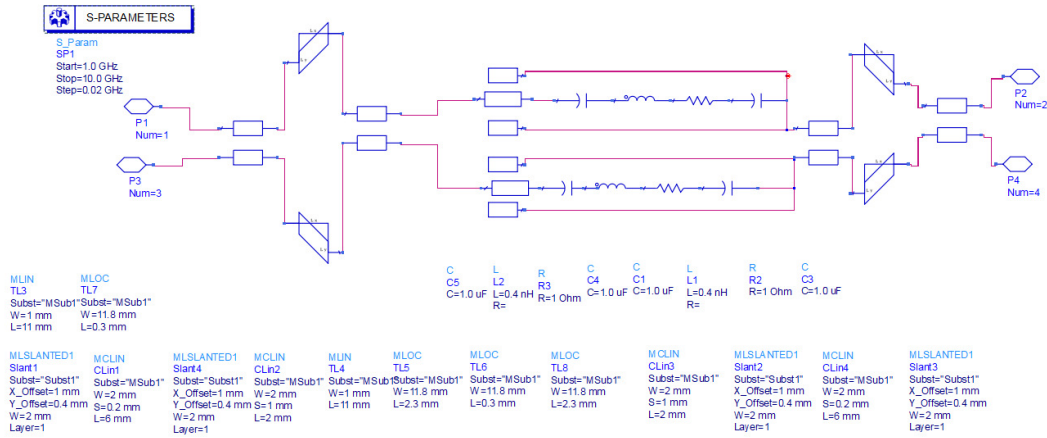


**FIGURE 8** Schematic diagram of equivalent CPS filter structure with PIN Diode

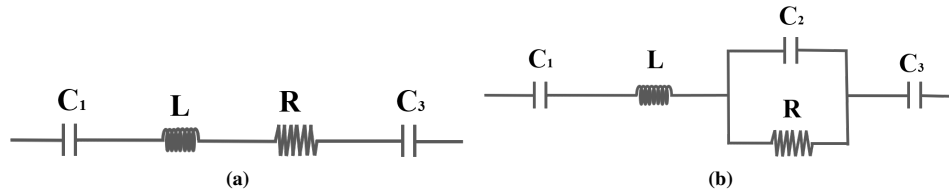


**FIGURE 9** Equivalent circuit of PIN diode (a) Forward biased (b) Reversed biased

**TABLE 4** Switching configurations of the proposed filter

| State | D1 | D2 | Operating frequency (GHz) |
|-------|----|----|---------------------------|
| 1     | FB | RB | 1-2.1, 4.8-5.3, 6.9-9     |
| 2     | RB | FB | 1-2.1, 4.8-5.3, 6.9-9     |
| 3     | RB | RB | 1.7-4.5, 7.5-9            |
| 4     | FB | FB | 6.7-9.1                   |

Four key clusters of the frequency range: 1- 2.1 GHz, 2.2-4.8 GHz, 4.9 - 5.3 GHz, and 6.9-9 GHz are covered for different combinations of states of the PIN diode arrangements. The impedance at the gap fails to yield good isolation at frequencies beyond the above-said ranges. The slot gap can be increased to decrease the coupling capacitance. However, an increment in inductance from the diode ultimately limits the effect of the enhanced separation gap. The RLC lumped element for PIN diode values are chosen as follows: C1=1uF, C2= 0.5pF, C3=1uF, L= 1.5 nH, R=1Ω for forward bias and reverse biased R2= 20 KΩ.

## 6 | RESULT AND DISCUSSION

The proposed work investigated the performances of the wideband BPF with PIN diodes. Analysis shows that the characteristic impedances to feeding CPS at the two ends are 112.3Ω with a coupling coefficient of 1.409. In contrast, for the slanted CPS, the impedance is 172.4Ω with a coupling coefficient of 1.323. The third-order and second-order BPF with PIN diodes offer a peak IL of 0.53 dB and RL of more than 13 dB at the operating frequency band of 1.7-5.9 GHz (FBW of 110%). The Fabricated prototype and filter under test are shown in Figure 10 . Figure 11 shows the comparison of losses with Real and Ideal PIN

diode. The scattering parameter performance of the closed and open ended cps spurline are shown in Figure 12 , and Figure 13 shows the scattering parameters performance of CPS with embedded PIN diode. The proposed filter results in the band pass and band rejection having a 2<sup>nd</sup> and 3<sup>rd</sup> orders when in both the open and closed conditions, as well as in the ON and OFF states of the PIN diode. Figure 14 shows the fabricated CPS filter with integrated PIN diode and reflections response for various diode states.

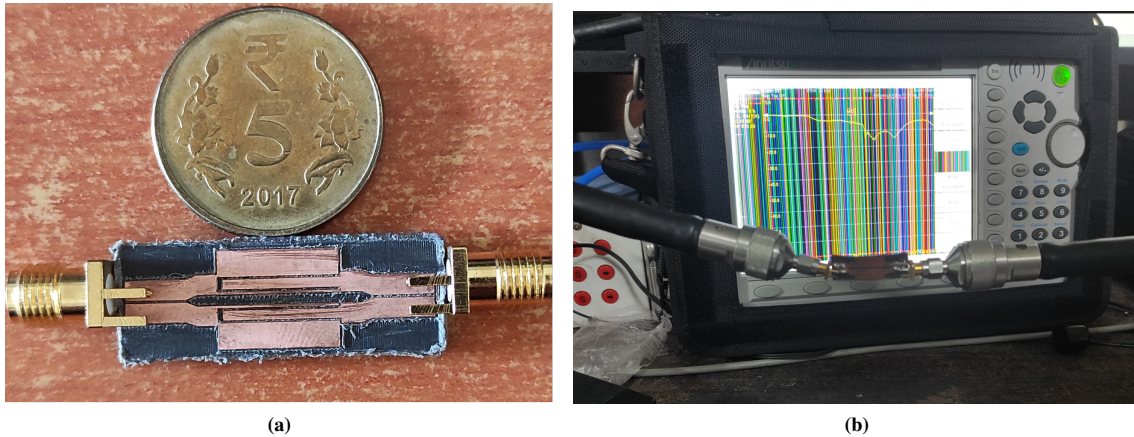


**FIGURE 10** Proposed filter (a) Fabricated prototype (b) Filter under test

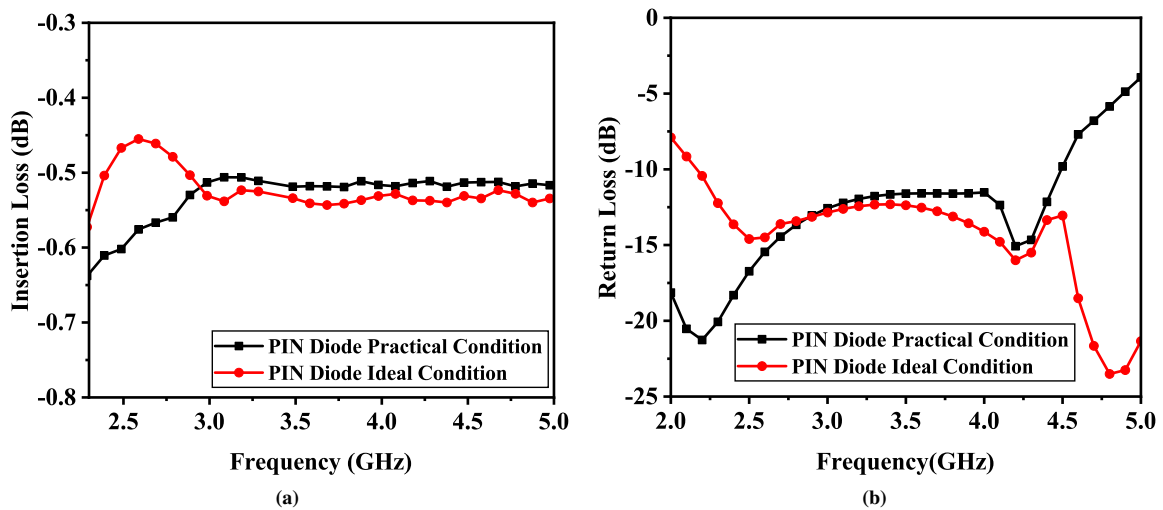


**FIGURE 11** Comparison of losses with Real and Ideal PIN diode (a) Insertion Loss (IL) (b) Return loss(RL)

To balance out the in-phase currents, the stub width for the parallel spurline in CPS is slanted and extended. Furthermore, in<sup>3</sup> a circular patch and a air bridge are used to mitigate the undesired even mode impact in the series stub CPS. Most of the previous investigations reported on first-order bandpass filters with restricted bandwidth. However, in our proposed design, the series spurline stub resonator is slightly slanted, and the stub width is enlarged to yield the second and third order BPF as shown in Figure 12 and Figure 13 . The S-parameters obtained using the series spurline stub structures with PIN diode in different conditions are presented in Figure 13 and Figure 14 . As in Figure 12 (a) and Figure 13 (a), the S-parameters for closed-ended and forward-biased diode state in ideal and practical conditions are almost identical, with two transmission zeros.

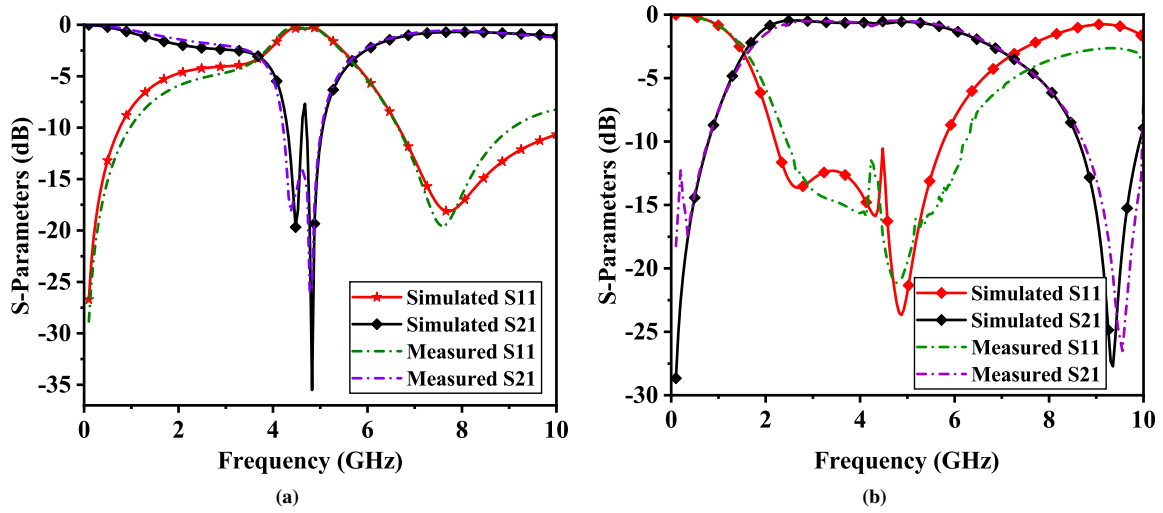


FIGURE 12 S-parameters of CPS filter configuration when (a) Closed-ended (b) Open-ended

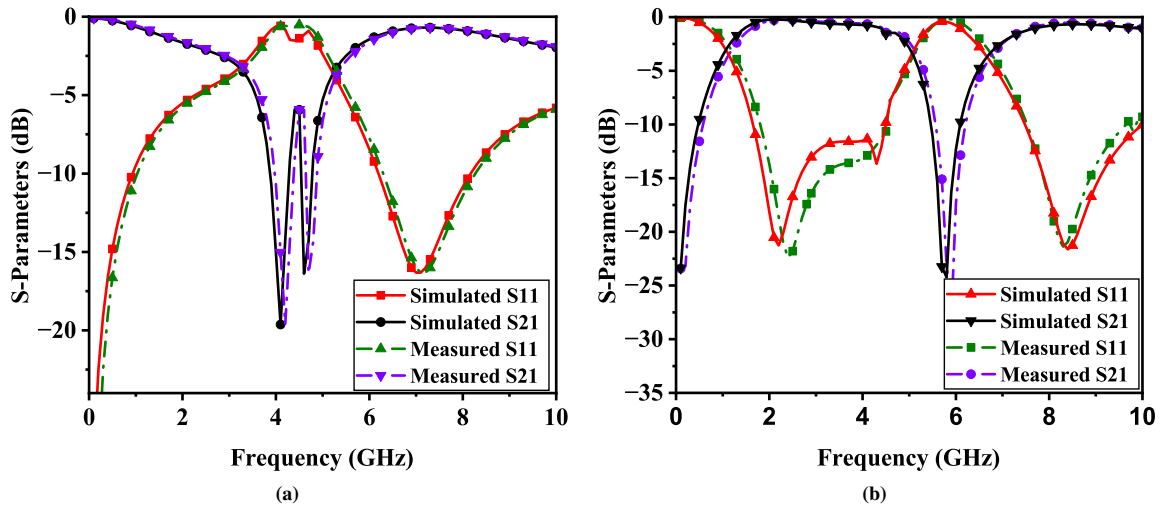
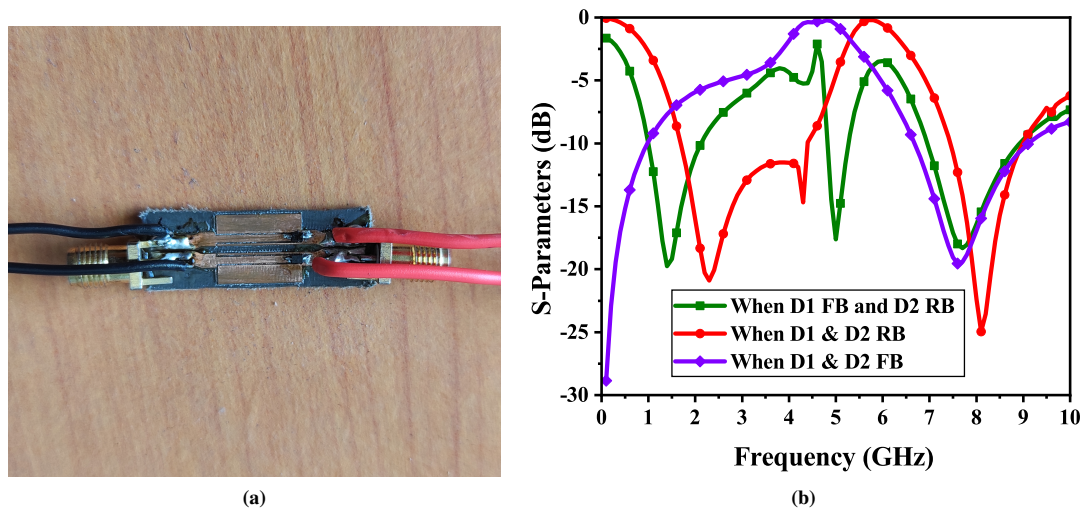


FIGURE 13 S-parameter for CPS when both PIN diode (D1,D2) in (a) Forward biased (b) Reversed biased

In our research work, we observed that as the stub wide is increased from  $W1 = 0.3$  to  $2.3$  mm, a sharp increase in selectivity up to  $37$  dB is found in the lower and upper bands of the filter response, as presented in Figure 12 and Figure 13 respectively. However, for the open-ended (reverse biased) structure, we obtained  $2^{nd}$  order, and the operating frequency ranges shrink from  $1.7$ -  $5.9$  GHz band to  $1.7$ - $4.9$  GHz as in Figure 13 (b). When the open-ended circuit stub length is  $12$  mm ( $\lambda/4$ ), a passband is obtained at  $4$  GHz. In the presented work, we have reduced the stub length to  $5$ mm ( $\lambda/10$ ) and the equivalent frequency results, as shown in Figure 12 (a), are compensated with the parasitic inductance and capacitance obtained by optimizing the G3. In the short-ended circuit, the stub will attain the stopband in case the stub length is  $(\lambda/4)$  ( $12$ mm). However, by adjusting the G3 the stop band is achieved with reduced dimension as in Figure 12 (b). Due to optimization, we receive one more pass band above  $7.5$  GHz for the open-ended condition, which is considered as the odd-mode second harmonic stub resonance. The article has accurately modeled the short and open-ended CPS spurline stub in the range of frequency from  $4$ - $10$  GHz and presented the parasitic components associated in Table 3. The analogous circuit depicted in Figure 6 (b) is a model for open-ended CPS spurline stub resonating over the frequencies range from  $5$  GHz to first passband resonance. The relevant relationships



**FIGURE 14** CPS structure with (a) Embedded PIN diode (b) S-parameter of PIN Diode in diversese state

have indeed been obtained that can provide values for the lumped components as a function of the stub length  $L_4$ . The proposed design filter has the smallest size, largest bandwidth, and minimum in-band IL as brief in Table 5 .

**TABLE 5** Comparison of the Performance of the final filter designed in this article with other references

| Ref.      | Series Stub type              | Order | Maximum in-band IL (dB) | Additional Features                                      | Frequency Band $f_0$ (GHz) | Sizes(mm) <sup>2</sup> |
|-----------|-------------------------------|-------|-------------------------|--|----------------------------|------------------------|
| 3         | CPS and Slotline dual stub    | 1     | 1.5                     | Wire bond/ Airbridge                                     | 5/9.8                      | 15 20                  |
| 11        | CPS/DSPSL and CPS single stub | 2/3   | 3.4/5.9                 | No stub binding  | 2.4                        | 30 50                  |
| 12        | CPS                           | 3     | 18/22                   | Double split ring resonators                             | 5.33/4.76                  | 10 10                  |
| 13        | CPS                           | 5/7   | 3.1/14.7                | Double-sided shunt-stub structure                        | 0.89-3.11                  | 35 130                 |
| 16        | Microstrip to CPS type        | 5     | <2.90                   | SL-stub vertical coupling                                | 0.8-3                      | 30 160                 |
| 18        | CPS spurline resonator        | 1/2   | 1.2                     | Wire-bond/Air bridges with PIN diode                     | 3.25                       | 15 25                  |
| 22        | CPS-Based MMRs in duality     | 5     | 0.85/2.70               | MMRs structure   | 1.83                       | 30 170                 |
| 25        | CPW Feed CPS dual stub        | 3/5   | 1.5/2.8                 | CPW feeding  | 1.11-2.98                  | 30 50                  |
| This work | CPS Multi Stub                | 3/2   | 0.54/0.51               | Enlarging the stub structureOn each side of the CPS line | 1.9/2.4/5/8                | 10 30                  |

## 7 | CONCLUSION

This study has adequately characterized the CPS spurline stubs and explored a simple design that does not require using a wire bond or an airbridge to suppress the parasitic modes. It efficiently slanted the CPS structure by an angle and enlarged the two-sided stub, and achieved frequency reconfigurability. The OFF/ON stages of the integrated PIN diodes on CPS spurline make the filter open and short-ended. The forward-biased PIN diodes make the CPS structure short-ended, resulting in a passband at 6.9-9 GHz. Similarly, the reverse-biased PIN diode makes the CPS spurline open-ended with resonant frequency at 1.7 - 4.9 GHz and 7.5-9 GHz. Moreover, with one of the diodes forward-biased and the other reverse-biased, it resonates at 1-2.1 GHz, 4.8-5.3 GHz, and 6.9-9 GHz with an insertion loss of below 0.55 dB.

## References

1. Knorr J, Kuchler K. Analysis of Coupled Slots and Coplanar Strips on Dielectric Substrate. *IEEE Transactions on Microwave Theory and Techniques* 1975; 23(7): 541-548.

2. Zhang X, Wu Y, Yu H, Wang W, Yang Y, Gao J. High selectivity wideband bandpass filters based on flexibly transferring the structure of a coupled-line. *AEU-International Journal of Electronics and Communications* 2022; 155: 154334.
3. Ponchak GE. Coplanar stripline spurline stub resonators with even-mode suppression for bandpass and bandstop filters. *IEEE Microwave and Wireless Components Letters* 2018; 28(12): 1098–1100.
4. Han C, Tang D, Deng Z, Qian HJ, Luo X. Filtering Power Divider With Ultrawide Stopband and Wideband Low Radiation Loss Using Substrate Integrated Defected Ground Structure. *IEEE Microwave and Wireless Components Letters* 2021; 31(2): 113–116.
5. Hazarika B, Basu B, Nandi A. A wideband, compact, high gain, low-profile, monopole antenna using wideband artificial magnetic conductor for off-body communications. *International Journal of Microwave and Wireless Technologies* 2022; 14(2): 194–203.
6. Laskar MI, Basu B, Nandi A. A multiband slot antenna with groundless EBG structure for wearable WLAN/WiMAX applications. *International Journal of Electronics* 2023: 1–16.
7. Martel J, Fernández-Prieto A, Río dJLM, Martín F, Medina F. Design of a differential coupled-line directional coupler using a double-side coplanar waveguide structure with common-signal suppression. *IEEE Transactions on Microwave Theory and Techniques* 2020; 69(2): 1273–1281.
8. Feng LP, Zhu L, Zhang S. Differential-mode low-pass filter using hybrid CPS and G-CPS with intrinsic common-mode rejection. *IEEE Transactions on Microwave Theory and Techniques* 2019; 67(5): 1836–1843.
9. Feng LP, Zhu L, Zhang S, Zhang X. Compact Chebyshev Differential-Mode Bandpass Filter on  $\lambda/2$  CPS Resonator With Intrinsic Common-Mode Rejection. *IEEE Transactions on Microwave Theory and Techniques* 2018; 66(9): 4047–4056.
10. Ouyang ZA, Zhu L, Qiu LL, Feng LP. Proposal of coplanar stripline series stub structure for wideband bandpass filters. *IEEE Transactions on Microwave Theory and Techniques* 2020; 68(8): 3397–3407.
11. Ponchak GE. Coplanar stripline coupled to planar double split-ring resonators for bandstop filters. *IEEE Microwave and Wireless Components Letters* 2018; 28(12): 1101–1103.
12. Ouyang ZA, Zhu L, Qiu LL. Wideband balanced filters with intrinsic common-mode suppression using coplanar strip double-sided shunt-stub structures. *IEEE Transactions on Microwave Theory and Techniques* 2021; 69(8): 3770–3782.
13. Ouyang ZA, Zhu L, Qiu LL. Wideband balanced-to-balanced microstrip-to-coplanar strip transitions with intrinsic common-mode suppression. *IEEE Transactions on Microwave Theory and Techniques* 2021; 69(8): 3726–3736.
14. Ouyang ZA, Zhu L, Qiu LL. Wideband balanced filters with intrinsic common-mode suppression on coplanar stripline-based multimode resonators. *IEEE Transactions on Circuits and Systems I: Regular Papers* 2022; 69(6): 2263–2275.
15. Chen W, Wu Y, Wang W. Planar wideband high-selectivity impedance-transforming differential bandpass filter with deep common-mode suppression. *IEEE Transactions on Circuits and Systems II: Express Briefs* 2019; 67(10): 1914–1918.
16. Xu KD, Zhang F, Guo Y, Ye L, Liu Y. Spoof surface plasmon polaritons based on balanced coplanar stripline waveguides. *IEEE Photonics Technology Letters* 2019; 32(1): 55–58.
17. Dong G, Li S, Yang X. A tunable bandpass filter with extended passband bandwidth. *International Journal of Microwave and Wireless Technologies* 2022; 14(10): 1233–1240.
18. Holda ME, Ponchak GE, Tentzeris EM. Coplanar Stripline Single Pole Single Throw Switch. *IEEE Microwave and Wireless Technology Letters* 2023.
19. Sreelakshmi K. Compact ACS-fed frequency reconfigurable octa-band antenna for wireless portable systems. *International Journal of Numerical Modelling: Electronic Networks, Devices and Fields* 2024: e3166.

20. Orugu R, Moses N. Triangular fractal loaded reconfigurable antenna with notch band characteristics. *International Journal of Numerical Modelling: Electronic Networks, Devices and Fields* 2021; 34(1): e2806.
21. Gómez-García R, Yang L, Muñoz-Ferreras JM, Psychogiou D. Single/multi-band coupled-multi-line filtering section and its application to RF diplexers, bandpass/bandstop filters, and filtering couplers. *IEEE Transactions on Microwave Theory and Techniques* 2019; 67(10): 3959–3972.
22. Lee JS, Min BC, Kumar S, Choi HC, Kim KW. On Autonomous Phase Balancing of the Coplanar Stripline as a Feedline for a Quasi-Yagi Antenna. *Electronics* 2023; 12(19): 4168.
23. Chen Y, Lu G, Wang S, Wang J. Coplanar Stripline-Fed Wideband Yagi Dipole Antenna with Filtering-Radiating Performance. *Electronics* 2020; 9(8): 1258.
24. Duan J, Zhu L. A Compact Narrow-Width Endfire Leaky Wave Antenna on Coplanar Stripline. *IEEE Transactions on Antennas and Propagation* 2022; 70(4): 3011-3016.
25. Ouyang ZA, Qiu LL, Zhu L. Coplanar waveguide-serially-connected coplanar strip dual stub structure for wideband bandpass filters. *International Journal of RF and Microwave Computer-Aided Engineering* 2021; 31(4): e22571.

